Journal of Sound and Vibration (1998) **211**(2), 179–194

THE 1:1 INTERNALLY RESONANT RESPONSE OF A CANTILEVER BEAM ATTACHED TO A ROTATING BODY

K. D. MURPHY

Department of Mechanical Engineering, University of Connecticut, Storrs, Connecticut 06269-3139, *U.S.A.*

AND

C. L. LEE

Structural Mechanics Group, Lawrence Livermore National Laboratory, Livermore, California 94551, *U.S.A.*

(*Received* 10 *March* 1997, *and in final form* 24 *September* 1997)

Modal coupling in the dynamics of a cantilever beam attached to a rotating body is investigated using a coupled, non-linear three-degree-of-freedom model which includes the effects of centrifugal stiffening. The near-resonant response of two lateral modes (one in-plane and one out-of-plane as defined by the plane of rotation) driven by a periodic out-of-plane excitation is examined for the case in which the natural frequencies of the lateral modes are commensurate in a near one-to-one ratio. The existence and stability of periodic solutions are examined using a second order perturbation analysis. Regions in the system parameter space are identified where single- or multi-mode responses may occur. Typical responses involve Hopf, saddle node and pitchfork bifurcations.

© 1998 Academic Press Limited

1. INTRODUCTION

The accurate dynamic simulation of rotating, flexible bodies such as rotor blades, robotic arms and satellite appendages requires models that correctly capture the effects of angular rotation. Extensive study in this area has resulted in a variety of non-linear continuum models; see, for example, references [1]–[8]. Correct formulations account for the angular rotation by including the centrifugal stiffening effect. In these models, equations governing motion in the axial and lateral directions are coupled through non-linear displacement terms. Models discretized using appropriate shape functions are likewise coupled.

Geometrically non-linear models of systems such as beams [9, 10], cables [11] and strings [12] have similar coupling terms. These systems have been shown to exhibit internally resonant responses in which modes of vibration that have (near) commensurate natural frequencies strongly couple. In stationary beams, a particular class of modal interactions can be excited because the natural frequencies of lateral modes are equal [9]. As will be shown in the case of a beam attached to a rotating body, this same class of internally resonant responses can also be excited for beams with particular cross-sections due to the centrifugal stiffening effect.

0022–460X/98/120179 + 16 $25.00/0/sv971341 © 1998 Academic Press Limited

In this study, the forced response of a cantilever beam attached to a rigid body rotating with constant angular velocity is examined using a three-degree-of-freedom model that represents axial, lateral in-plane and lateral out-of-plane motion. The model, which contains both quadratic and cubic non-linearities, includes the effects of centrifugal stiffening and gyroscopic coupling. Beam cross-section configurations as functions of rotation speed are determined for which the natural frequencies of the in-plane and out-of-plane (as defined by the plane of rotation of the beam) modes appear in a (near) 1 : 1 ratio. Typical near-resonant responses in the two lateral directions driven by an applied periodic, out-of-plane excitation are presented for these configurations. A second-order perturbation analysis is used to determine the existence and stability of weakly non-linear periodic motion. Loci of system parameters at which 1:1 internally resonant responses bifurcate from single-degree-of-freedom responses are determined from the state equations that govern stability.

2. CONTINUUM MODEL

Illustrated in Figure 1 is a flexible cantilever beam attached to a rigid body of radius R which rotates with a constant angular speed, ω, about a body axis that is fixed in inertial space. The beam is uniform, with length L, cross-sectional area A ($= a \times b$), density ρ, mass per unit length m and Young's modulus E. For reference, the point O is located on the elastic axis of the beam at the intersection of the beam and the rigid body. The deflection of an arbitrary point P, which lies in a generic cross-section in the undeformed state, is given by $\mathbf{r}^{OP} = (x + U)\mathbf{a}_1 + (y + v)\mathbf{a}_2 + (z + w)\mathbf{a}_3$, where the unit vector triad $(\mathbf{a}_1, \mathbf{a}_2, \mathbf{a}_3)$ is fixed with respect to the rigid body. The displacement co-ordinates (U, v, w) and distances (x, y, z) are respectively aligned with $(\mathbf{a}_1, \mathbf{a}_2, \mathbf{a}_3)$. From Navier's hypothesis for beams, the total axial displacement $U(x, t)$ can be expressed as a sum of the axial stretching and the in-plane displacements due to bending as $U(x, t) = -yv_{,x}(x, t) - zw_{,x}(x, t) + u(x, t)$. Here, $u(x, t)$ is the stretching displacement in the x-direction of point P, t is time and $()_{,x} \equiv \mathrm{d}()/\mathrm{d}x$.

The kinetic energy, KE, of the deformed configuration is

$$KE = \tfrac{1}{2}\int_0^L \{m(\dot{u}^2 + \dot{v}^2 + \dot{w}^2) + m\omega^2 v^2 - 2m\omega\dot{u}v + 2m\omega x\dot{v} + 2m\dot{v}u\omega + m\omega^2 x^2$$

$$+ \rho I_z \omega^2 + m\omega^2 u^2 + 2m\omega^2 xu + m\omega^2 R^2 + 2m\omega R\dot{v} + 2m\omega^2 Rx + 2m\omega^2 Ru\}\,\mathrm{d}x, \quad (1)$$

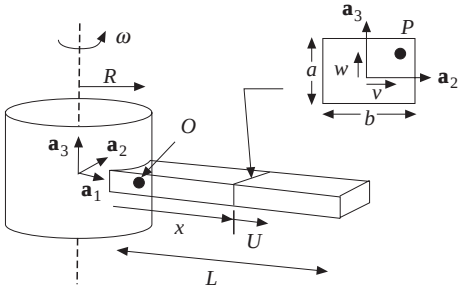

Figure 1. The flexible beam is affixed to a rigid, central hub of radius R. The beam has uniform properties including the Young's modulus E and mass per unit length m.

where the following assumptions are applied: the center of gravity remains on the centroidal axis; the cross-sectional area is symmetric, the axes of the beam are the principal axes; rotary inertia and shear effects are negligible; and torsional motion is not considered.

The potential energy, PE is formulated using Euler–Bernoulli beam theory and a non-linear strain–displacement relationship. Furthermore, the beam is a one-dimensional, elastic continuum obeying a linear stress–strain relationship. Using the von Kármán strain measure, $\epsilon_{xx} = (u_{,x} + \frac{1}{2} v_{,x}^2 + \frac{1}{2} w_{,x}^2)$, the potential energy is

$$PE = \tfrac{1}{2} \int_0^L E(I_z v_{,xx}^2 + I_y w_{,xx}^2)\, \mathrm{d}x + \tfrac{1}{2} \int_0^L EA(u_{,x} + \tfrac{1}{2} v_{,x}^2 + \tfrac{1}{2} w_{,x}^2)^2\, \mathrm{d}x, \tag{2}$$

where I_y and I_z are the area moments of inertia about the $\mathbf{a}_2$- and $\mathbf{a}_3$-axes, respectively. Note that the term $\frac{1}{2} u_{,x}^2$ in the axial strain is considered to be small in comparison to $u_{,x}$.

Application of Hamilton's Principle leads to the coupled, three-dimensional, non-linear equations of free motion:

$$-m\ddot{u} + 2m\omega\dot{v} + m\omega^2 u + m\omega^2(x + R) + EA[u_{,x} + \tfrac{1}{2} v_{,x}^2 + \tfrac{1}{2} w_{,x}^2]_{,x} = 0, \tag{3}$$

$$-m\ddot{v} - 2m\omega\dot{u} + m\omega^2 v - EI_z v_{,xxxx} + EA[(u_{,x} + \tfrac{1}{2} v_{,x}^2 + \tfrac{1}{2} w_{,x}^2)v_{,x}]_{,x} = 0, \tag{4}$$

$$-m\ddot{w} - EI_y w_{,xxxx} + EA[(u_{,x} + \tfrac{1}{2} v_{,x}^2 + \tfrac{1}{2} w_{,x}^2)w_{,x}]_{,x} = 0. \tag{5}$$

Note that the equations of motion allow for axial/bending coupling and that motions in the u and v directions are coupled gyroscopically. The accompanying boundary conditions are

$$u(0, t) = v(0, t) = w(0, t) = 0, \qquad v_{,x}(0, t) = w_{,x}(0, t) = 0,$$

$$u_{,x}(L) + \tfrac{1}{2} v_{,x}^2(L) + \tfrac{1}{2} w_{,x}^2(L) = 0,$$

$$I_y w_{,xx}(L) + I_z v_{,xx}(L) = 0, \qquad I_y w_{,xxx}(L) + I_z v_{,xxx}(L) = 0. \tag{16}$$

3. DISCRETE MODEL

Modal interactions between motions in the transverse directions are investigated using a three-degree-of-freedom model. The equations of motion of the continuum model are discretized using the separable solutions

$$u(x, t) = \Upsilon_i(x)\alpha(t), \qquad v(x, t) = \Psi_i(x)\beta(t), \qquad w(x, t) = \Phi_i(x)\gamma(t), \tag{7}$$

where the spatial functions, $\Upsilon_i(x)$, $\Psi_i(x)$ and $\Phi_i(x)$ are the ith eigenfunctions corresponding to vibrations in the axial, and two lateral directions, respectively, for an Euler–Bernoulli beam with fixed–free boundary conditions rotating at a constant speed. These eigenfunctions can be calculated numerically from properly linearized equations of motion corresponding to equations (3)–(5). For low speeds, the eigenfunctions corresponding to a non-rotating Euler–Bernoulli beam with fixed–free boundary conditions may be satisfactory.

Taking $i = 1$, substitution of equations (7) into equations (3)–(5) and application of Galerkin's method leads to the three-degree-of-freedom, discrete model

$$\ddot{\alpha} + 2\zeta_a \omega_a \dot{\alpha} + A_1 \dot{\beta} + \omega_a^2 \alpha + A_3 + A_4 \beta^2 + A_5 \gamma^2 = 0, \tag{8}$$

$$\ddot{\beta} + 2\zeta_b \omega_b \dot{\beta} + B_1 \dot{\alpha} + \omega_b^2 \beta + B_3 \alpha\beta + B_4 \gamma^2\beta + B_5 \beta^3 = 0, \tag{9}$$

$$\ddot{\gamma} + 2\zeta_c \omega_c \dot{\gamma} + \omega_c^2 \gamma + C_2 \alpha\gamma + C_3 \beta^2\gamma + C_4 \gamma^3 = F \cos(\Omega t/\omega), \tag{10}$$

where modal damping terms have been introduced. In addition, a forced, periodic excitation of amplitude, F, and frequency, Ω, has been applied in the out-of-plane direction. F represents the spatial variation of the applied force as projected on to Φ_1. The (constant) coefficients in the above equations are calculated in the standard manner.

An important observation is that ω_b is *not* the natural frequency of the beam since it only captures the contributions from the terms $m\omega v - EI_z v_{,xxxx}$. The "full rotating frequency", later called κ_b, will also have a contribution from the $-m\omega^2(x+R)$ term in the u equation.

4. PERTURBATION ANALYSIS: PERIODIC SOLUTIONS

Periodic solutions to equations (8)–(10) are found for the weakly non-linear response near primary resonance of the out-of-plane (lateral) mode. Solutions are determined up to second non-linear order using a multiple scales perturbation method following references [11] and [16].

To begin, four independent time scales are defined in terms of a small (positive) parameter, ϵ, as follows:

$$T_n = \epsilon^n(\Omega/\omega)\tau, \qquad n = 0, 1, 2, 3, \tag{11}$$

where T_0 is a quasi-static time scale, T_1 is a "fast" or linear time scale, and T_2 and T_3 are "slow" time scales that capture the effects of the non-linearities, damping, gyroscopic coupling and external excitation. Derivative operators on the original time scale, t, may be expressed in terms of the new time scales using the chain rule as

$$\frac{\mathrm{d}}{\mathrm{d}t} = (\Omega/\omega)\,[D_0 + \epsilon D_1 + \epsilon^2 D_2 + \cdots],$$

$$\frac{\mathrm{d}^2}{\mathrm{d}t^2} = (\Omega/\omega)^2[D_0^2 + 2\epsilon D_0 D_1 + \epsilon^2 D_1^2 + 2\epsilon^2 D_0 D_2 + \cdots]. \tag{12}$$

The modal displacement amplitudes are expanded, to second nonlinear order $O(\epsilon^3)$, as a uniform expansion in the new time scales,

$$\alpha = \alpha_0 + \sum_{n=1}^{3} \epsilon^n \alpha_n\,(T_1, T_2, T_3),$$

$$\beta = \sum_{n=1}^{3} \epsilon^n \beta_n\,(T_1, T_2, T_3), \qquad \gamma = \sum_{n=1}^{3} \epsilon^n \gamma_n\,(T_1, T_2, T_3). \tag{13}$$

The constant term α_0 has been added to the axial displacement term, α, in order to account for the quasi-static stretching of the beam as it rotates. This stiffening effect appears in the equations of motion as $-m\omega^2(x+R)$ which is constant for a fixed rotation speed ω. Note that α_0 is a static term of $O(1)$ and is consequently an order of magnitude larger than the axial motion on the $O(\epsilon^1)$ time scale.

In addition, the excitation amplitude and the damping coefficients are ordered so that they appear at the first non-linear order:

$$F = \epsilon^2 F_1 + \epsilon^3 F_2, \tag{14}$$

$$2\zeta_a\,\omega_a\,(\Omega/\omega) = \epsilon\mu_{a1} + \epsilon^2\mu_{a2}, \qquad 2\zeta_b\,\omega_b\,(\Omega/\omega) = \epsilon\mu_{b1} + \epsilon^2\mu_{b2},$$

$$2\zeta_c\,\omega_c\,(\Omega/\omega) = \epsilon\mu_{c1} + \epsilon^2\mu_{c2}. \tag{15}$$

Likewise, the gyroscopic terms are ordered as

$$A_1(\Omega/\omega) = \epsilon v_{a1} + \epsilon^2 v_{a2}, \qquad B_1(\Omega/\omega) = \epsilon v_{b1} + \epsilon^2 v_{b2}. \tag{16}$$

For the case in which the natural frequencies of the (lateral) in-plane mode and the out-of-plane mode are nearly equal, their relationship can be expressed as

$$\kappa_b = \kappa_c + \epsilon\sigma_2, \tag{17}$$

where κ_b and κ_c are the *full rotating natural frequencies* of the respective modes. These frequencies differ from the frequencies ω_b and ω_c, as will be described shortly. The term σ_2 is the internal detuning parameter.

The external excitation frequency is applied for the case of primary resonance of the out-of-plane mode and is expanded as

$$(\Omega/\omega)^2 = \kappa_c^2 + \epsilon\sigma_{11} + \epsilon^2\sigma_{12}, \tag{18}$$

where σ_{11} and σ_{12} are external detuning parameters.

Equations (11)–(18) are substituted into the discretized equations of motion (8)–(10), and terms with like powers of ϵ are collected as the quasi-static, $O(\epsilon^0)$; linear, $O(\epsilon^1)$; first non-linear, $O(\epsilon^2)$; and second non-linear, $O(\epsilon^3)$; order equations below;

Order ϵ^0:

$$A_3 + \omega_a^2\,\alpha_0 = 0. \tag{19}$$

Order ϵ^1:

$$\kappa_c^2 D_0^2\,\alpha_1 + \omega_a^2\,\alpha_1 = 0, \qquad \kappa_c^2 D_0^2\,\beta_1 + (\omega_b^2 + \alpha_0 B_3)\beta_1 = 0, \tag{20, 21}$$

$$\kappa_c^2 D_0^2\,\gamma_1 + (\omega_c^2 + \alpha_0 C_2)\gamma_1 = 0. \tag{22}$$

Order ϵ^2:

$$\kappa_c^2 D_0^2\,\alpha_2 + \omega_a^2\,\alpha_2 = -A_4\,\beta_1^2 - A_5\,\gamma_1^2 - \sigma_{11} D_0^2\,\alpha_1 - 2\kappa_c^2 D_0 D_1\,\alpha_1 - \mu_{a1} D_0\,\alpha_1 - v_{a1} D_0\,\beta_1, \tag{23}$$

$$\kappa_c^2 D_0^2\,\beta_2 + (\omega_b^2 + \alpha_0 B_3)\beta_2 = -\alpha_1\,\beta_1\,\beta_3 - \sigma_{11} D_0^2\,\beta_1 - 2\kappa_c^2 D_0 D_1\,\beta_1 - \mu_{b1} D_0\,\beta_1 - v_{b1} D_0\,\alpha_1, \tag{24}$$

$$\kappa_c^2 D_0^2\,\gamma_2 + (\omega_c^2 + \alpha_0 C_2)\gamma_2 = -\alpha_1 C_2\,\gamma_1 - \sigma_{11} D_0^2\,\gamma_1 - 2\kappa_c^2 D_0 D_1\,\gamma_1 - \mu_{c1} D_0\,\gamma_1 + F_1\cos(T_0). \tag{25}$$

Order ϵ^3:

$$\begin{aligned}\kappa_c^2 D_0^2\,\alpha_3 + \omega_a^2\,\alpha_3 = {} & -2A_4\,\beta_1\,\beta_2 - A_5\,\gamma_1\,\gamma_2 - 2\kappa_c^2 D_0 D_1\,\alpha_2 - \kappa_c^2 D_1^2\,\alpha_1 - 2\kappa_c^2 D_0 D_2\,\alpha_1 \\ & - \mu_{a1} D_0\,\alpha_2 - \mu_{a1} D_1\,\alpha_1 - \mu_{a2} D_0\,\alpha_1 - v_{a1} D_0\,\beta_2 - v_{a1} D_1\,\beta_1 - v_{a2} D_0\,\beta_1 \\ & - \sigma_{11} D_0^2\,\alpha_2 - 2\sigma_{11} D_0 D_1\,\alpha_1 - \sigma_{11} D_1^2\,\alpha_0 - \sigma_{12} D_0^2\,\alpha_1,\end{aligned} \tag{26}$$

$$\begin{aligned}\kappa_c^2 D_0^2\,\beta_3 + (\omega_b^2 + \alpha_0 B_3)\beta_3 = {} & -B_3\,\alpha_2\,\beta_1 - B_3\,\alpha_1\,\beta_2 - B_5\,\beta_1^3 - B_4\,\beta_1\,\gamma_1^2 - 2\kappa_c^2 D_0 D_1\,\beta_2 \\ & - \kappa_c^2 D_1^2\,\beta_1 - 2\kappa_c^2 D_0 D_2\,\beta_1 - \mu_{b1} D_0\,\beta_2 - \mu_{b1} D_1\,\beta_1 - \mu_{b2} D_0\,\beta_1 - v_{b1} D_0\,\alpha_2 \\ & - v_{b1} D_1\,\alpha_1 - v_{b2} D_0\,\alpha_1 - \sigma_{11} D_0^2\,\beta_2 - 2\sigma_{11} D_0 D_1\,\beta_1 - \sigma_{12} D_0^2\,\beta_1,\end{aligned} \tag{27}$$

$$\begin{aligned}\kappa_c^2 D_0^2\,\gamma_3 + (\omega_c^2 + \alpha_0 C_2)\gamma_3 = {} & -C_2\,\alpha_2\,\gamma_1 - C_3\,\beta_1^2\,\gamma_1 - C_4\,\gamma_1^3 - C_2\,\alpha_1\,\gamma_2 - \kappa_c^2 D_1^2\,\gamma_1 - 2\kappa_c^2 D_0 D_2\,\gamma_1 \\ & - 2\kappa_c^2 D_0 D_1\,\gamma_2 - \mu_{c1} D_1\,\gamma_1 - \mu_{c1} D_0\,\gamma_2 - \mu_{c2} D_0\,\gamma_1 - 2\sigma_{11} D_0 D_1\,\gamma_1 \\ & - \sigma_{11} D_0^2\,\gamma_2 - \sigma_{12} D_0^2\,\gamma_1 + F_2\cos(T_0).\end{aligned} \tag{28}$$

Consider the quasi-static $O(\epsilon^0)$ equation (19). The solution for α_0 is $-A_3/\omega_a^2$. Notice that A_3 is the Galerkin coefficient associated with the term $-m\omega^2(x+R)$. Hence, α_0 accounts for the axial stretching produced by the centrifugal stiffening which arises from the (constant) rotation speed of the rigid body.

Next, consider the three $O(\epsilon^1)$ equations. On the basis of the coefficients of the linear stiffness terms, the following definitions are made:

$$\kappa_a^2 = \omega_a^2, \qquad \kappa_b^2 = \omega_b^2 + \alpha_0 B_3, \qquad \kappa_c^2 = \omega_c^2 + \alpha_0 C_2. \tag{29–31}$$

The terms, κ_i, $i = a, b, c$ are referred to as the *full rotating natural frequencies* in their respective directions because they include an additional quantity arising from the increased stiffness due to axial stretching; i.e., α_0. Using the definitions

$$\eta_a = \kappa_a/\kappa_c, \qquad \eta_b = \kappa_b/\kappa_c,$$

the solution to equations (20)–(22) are

$$\alpha_1 = C_a(T_1, T_2)\,e^{i\eta_a T_0} + c.c., \qquad \beta_1 = C_b(T_1, T_2)\,e^{i\eta_b T_0} + c.c., \tag{32, 33}$$

$$\gamma_1 = C_c(T_1, T_2)\,e^{iT_0} + c.c., \tag{34}$$

where $c.c.$ indicates the complex conjugate of the preceding terms. The coefficients of these solutions are slowly varying (complex) amplitudes that will be determined from the $O(\epsilon^2)$ and $O(\epsilon^3)$ equations.

Solutions for α_2, β_2 and γ_2 are determined at $O(\epsilon^2)$ where the lower order solutions (α_0, α_1, β_1 and γ_1) act as excitation terms. By substituting equations (32–34) into equations (23–25), terms proportional to $e^{i\eta_a T_0}$, $e^{i\eta_b T_0}$ and e^{iT_0} in the α, β and γ equations, respectively, appear as non-homogeneous terms. These terms are *secular* and become unbounded as $t \to \infty$. Elimination of the secular terms leads to the following three state equations:

$$-2i\eta_a \kappa_c^2 D_1 C_a + \sigma_{11}\eta_a^2 C_a - i\mu_{a1}\eta_a C_a = 0, \tag{35}$$

$$-2i\eta_b \kappa_c^2 D_1 C_b + \sigma_{11}\eta_b^2 C_b - i\mu_{b1}\eta_b C_b = 0, \tag{36}$$

$$-2i\kappa_c^2 D_1 C_c + \sigma_{11} C_a - i\mu_{c1} C_a + \tfrac{1}{2} F_1 = 0. \tag{37}$$

Non-secular terms remain and extending the perturbation solution to the next order requires the particular solutions for α_2, β_2 and γ_2. These solutions are presented in Appendix A.

Following a similar procedure on $O(\epsilon^3)$, leads to the following state equations:

$$\begin{aligned} &-2i\eta_a \kappa_c^2 D_2 C_a - \mu_{a2} i\eta_a C_a + \nu_a \eta_a \Gamma_6 \nu_b C_a + \sigma_{21}\eta_a^2 C_a \\ &\quad - 2A_4(\Gamma_8 C_a \bar{C}_b C_b + \Gamma_7 C_a C_b \bar{C}_b) - 2A_5(\Gamma_{10} C_a \bar{C}_c C_c + \Gamma_9 C_a C_c \bar{C}_c) = 0, \end{aligned} \tag{38}$$

$$\begin{aligned} &-2i\eta_b \kappa_c^2 D_2 C_b - \mu_{b2} i\eta_b C_b + \nu_a \nu_b \eta_b \Gamma_1 C_b + \sigma_{12}\eta_b^2 C_b \\ &\quad - B_3(\Gamma_4 C_b^2 \bar{C}_b + \Gamma_5 C_c \bar{C}_c C_b + \Gamma_2 C_b^2 \bar{C}_b + \Gamma_3 C_c^2 \bar{C}_b\, e^{i(2(\sigma_{21}/\kappa_c)T_1)}) \\ &\quad - B_3 C_b C_a \bar{C}_a(\Gamma_8 + \Gamma_7) - 3B_5 C_b^2 \bar{C}_b - B_4(2C_c \bar{C}_c C_b + \bar{C}_b C_c^2\, e^{-i(2\sigma_{21}/\kappa_c)T_1}) = 0, \end{aligned} \tag{39}$$

$$\begin{aligned} &-2i\kappa_c^2 D_2 C_c - i\mu_{c2} C_c + \sigma_{12} C_c \\ &\quad - C_2(\Gamma_4 C_b \bar{C}_b C_c + \Gamma_5 C_c^2 \bar{C}_c + \Gamma_2 C_b^2 \bar{C}_c\, e^{i(2\sigma_{21}/\kappa_c)T_1} + \Gamma_3 C_c^2 \bar{C}_c) \\ &\quad - C_2 C_c C_a \bar{C}_a(\Gamma_9 + \Gamma_{10}) - C_3(2C_b \bar{C}_b C_c + C_b^2 \bar{C}_c\, e^{i(2\sigma_{21}/\kappa_c)T_1}) - 3C_4 C_c^2 \bar{C}_c + \tfrac{1}{2} F_2 = 0, \end{aligned} \tag{40}$$

where the overbar denotes a complex conjugate. It should be pointed out that equations (39) and (40) have small divisor terms proportional to $e^{i(2-\eta_b)T_0}$ and $e^{i(2\eta_b - 1)T_0}$, respectively.

These become secular due to the 1:1 internal resonance, equation (17). Furthermore, since the $O(\epsilon^2)$ secular terms describe modulations on the T_2 time scale only, they should be treated as independent of the T_1 time scale [16].

The complex response amplitudes (C_a, C_b, C_c) may be described in terms of the response amplitudes on the slower time scales: namely,

$$\dot{C}_k = \epsilon D_1 C_k + \epsilon^2 D_2 C_k, \qquad k = a, b, c, \tag{41}$$

where the overdot denotes a derivative with respect to the original time scale, t. The above three equations describe modulations of the complex displacement amplitudes on the original time scale. The terms $D_1 C_k$ and $D_2 C_k$ are obtained from the secular equations at order $O(\epsilon^2)$ (equations (35)–(37)) and at order $O(\epsilon^3)$ (equations (38)–(40)), respectively.

Approximate, steady state periodic solutions of (8)–(10) can be obtained from the singular points of an autonomous form of equation (41). Algebraic equations defining these points can be found by introducing the polar forms

$$C_a = \tfrac{1}{2} M_a (T_1, T_2)\, e^{i\phi_a(T_1,T_2)}, \qquad C_b = \tfrac{1}{2} M_b (T_1, T_2)\, e^{i\phi_b(T_1,T_2)}, \tag{42, 43}$$

$$C_c = \tfrac{1}{2} M_c (T_1, T_2)\, e^{i\phi_c(T_1,T_2)} \tag{44}$$

into equation (41), separating the real and imaginary parts, and setting all time derivatives on the original time scale to zero. This yields a set of six non-linear, algebraic state equations which can be solved numerically for M_a, M_b, M_c, ϕ_a, ϕ_b and ϕ_c using a multi-dimensional root finding algorithm. The state equations are shown below:

$$((\Omega/\omega)^2 - \kappa_c^2)\eta_a^2 M_a + A_1 B_1 (\Omega/\omega)^2 \eta_a \Gamma_6 M_a - \tfrac{1}{2} A_4 M_b^2 M_a (\Gamma_7 + \Gamma_8) - \tfrac{1}{2} A_5 M_a M_c^2 (\Gamma_9 + \Gamma_{10}) = 0, \tag{45}$$

$$2\zeta_a \omega_a (\Omega/\omega)\eta_a M_a = 0, \tag{46}$$

$$2\kappa_c \eta_b M_b (\kappa_b - \kappa_c) = ((\Omega/\omega)^2 - \kappa_c^2)\eta_b^2 M_b + A_1 B_1 (\Omega/\omega)^2 \eta_b \Gamma_1 M_b - \tfrac{1}{4} B_3 M_b^3 (\Gamma_2 + \Gamma_4) - \tfrac{3}{4} B_5 M_b^3 - \tfrac{1}{4} B_3 \Gamma_5 M_b M_c^2 - \tfrac{1}{4} B_3 \Gamma_3 M_b M_c^2 \cos(\theta) - \tfrac{1}{2} B_4 M_c^2 M_b - \tfrac{1}{4} B_3 M_a^2 M_b (\Gamma_7 + \Gamma_8) - \tfrac{1}{4} B_4 M_b M_c^2 \cos(\theta), \tag{47}$$

$$-2\zeta_b \omega_b (\Omega/\omega)\eta_b M_b + \tfrac{1}{4} B_3 \Gamma_3 M_b M_c^2 \sin(\theta) + \tfrac{1}{4} B_4 M_b M_c^2 \sin(\theta) = 0, \tag{48}$$

$$((\Omega/\omega)^2 - \kappa_c^2)M_c + F\cos(\phi_c) - \tfrac{1}{4} C_2 \Gamma_4 M_c M_b^2 - \tfrac{1}{4} C_2 M_c^3 (\Gamma_3 + \Gamma_5) - \tfrac{1}{4} C_2 \Gamma_2 M_b^2 M_c \cos(\theta) - \tfrac{1}{4} C_2 M_a^2 (\Gamma_9 + \Gamma_{10}) - \tfrac{1}{2} C_3 M_b^2 M_c - \tfrac{1}{4} C_3 M_b^2 M_c \cos(\theta) - \tfrac{3}{4} C_4 M_c^3 = 0, \tag{49}$$

$$-2\zeta_c \omega_c (\Omega/\omega)M_c - F\sin(\phi_c) - \tfrac{1}{4} C_2 \Gamma_2 M_b^2 M_c \sin(\theta) - \tfrac{1}{4} C_3 M_b^3 M_c \sin(\theta) = 0, \tag{50}$$

where θ is defined as $\theta = 2\phi_b - 2\phi_c + (2\sigma_{21}/\kappa_c)T_1$.

Note that, from equation (46), $M_a = 0$ for non-trivial system parameters and excitation. Furthermore, ϕ_a is arbitrary, since it does not appear in any of the state equations. Therefore, there is no dynamic component to the axial deformation; i.e., axial modes do not participate in the 1:1 internally resonant response of the lateral modes.

5. STABILITY OF PERIODIC SOLUTIONS

The fixed points of the state equations (equations (45)–(50)) correspond to periodic responses. The stability of these responses can be ascertained by applying small

perturbations to the periodic solutions and considering the local growth or decay of the perturbation. Consider

$$C_a = C_a^* + \delta C_a, \qquad C_b = C_b^* + \delta C_b, \qquad C_c = C_c^* + \delta C_c, \tag{51}$$

where C_i^* and δC_i $(i = a, b, c)$ are the periodic solutions and their respective small perturbations. These expressions are then substituted into the state equations which are then linearized. Three variational equations result. Using equations (42)–(44) and the definitions

$$\delta C_a = (p_r + \mathrm{i}p_i)\,\mathrm{e}^{\mathrm{i}\phi_a}\,\mathrm{e}^{\lambda T_0}, \qquad \delta C_b = (q_r + \mathrm{i}q_i)\,\mathrm{e}^{\mathrm{i}\Phi_b}\,\mathrm{e}^{\lambda T_0}, \qquad \delta C_c = (r_r + \mathrm{i}r_i)\,\mathrm{e}^{\mathrm{i}\phi_c}\,\mathrm{e}^{\lambda T_0}, \tag{52}$$

the three variational equations may be separated into real and imaginary parts yielding six equations governing stability.

As $M_a = 0$, the lateral stability equations uncouple from the axial equation allowing the axial stability to be determined independently. The real part of the axial motion eigenvalues is $\mathrm{Re}\,(\lambda_{1,2}) = -2\zeta_a\,\omega_a\,(\Omega/\omega)\eta_a\,/(2\kappa_c^2\,\eta_a)$, indicating asymptotic stability. The stability of the lateral oscillations (both in-plane and out-of-plane) are determined from the remaining 4×4 eigenvalue problem

$$[S]\mathbf{x} = \lambda\mathbf{x}, \tag{53}$$

where $\mathbf{x} = \{q_r, q_i, r_r, r_i\}^{\mathrm{t}}$ and the elements of the matrix $[S]$ are given in Appendix B.

6. RESULTS

6.1. CONDITIONS FOR 1:1 INTERNAL RESONANCE

It is first necessary to identify beam configurations in which the natural frequencies of the in-plane and out-of-plane modes are equal. Here, for simplicity, the beam cross-sections are taken to be rectangular ($A = a \times b$). Note that it is straightforward to extend the results to an arbitrary cross-section. For a stationary beam, the natural frequencies of the in-plane and out-of-plane modes are equal when the cross-section is square ($a = b$). This is not the case, however, when the beam is rotating. For non-zero rotation speeds, the natural frequencies of the out-of-plane modes are higher than those of the corresponding in-plane modes [13]. Since the influence of the centrifugal stiffness in each lateral direction is different, the beam cross-section must be rectangular in order for the natural frequencies to be equal. Specific combinations of cross-section (moment of inertia) and rotation speed for which this occurs can be calculated numerically from the linearized equations of motion (8)–(10) or approximated using the perturbation solution presented herein.

Equating the full rotating natural frequencies (30)–(31), $\kappa_c = \kappa_b$, leads to

$$C_2\,\alpha_0 + \omega_c^2 = B_3\,\alpha_0 + \omega_b^2. \tag{54}$$

As an example, the eigenfunctions of a non-rotating beam are chosen. The Galerkin coefficients C_2 and B_3 have the same form arising from $-k(U_{,x}\,V_{,x})_{,x}$ and $-k(U_{,x}\,W_{,x})_{,x}$. These terms cancel, leaving $\omega_c^2 = \omega_b^2$ or

$$\frac{EI_y}{m\omega^2 L^4}\,w_{,xxxx} = -v + \frac{EI_z}{m\omega^2 L^4}\,v_{,xxxx}. \tag{55}$$

If the first mode is considered, equation (55) becomes

$$\frac{EI_y}{m\omega^2 L^4}\,(1{\cdot}875)^4\Psi = -\Phi + \frac{EI_z}{m\omega^2 L^4}\,(1{\cdot}875)^4\Phi, \tag{56}$$

where $I_y = ba^3/12$, $I_z = ab^3/12$ and $m = \rho ab$. Rearranging, equation (56) gives

$$\frac{\rho\omega^2 L^2}{E} = \frac{(1{\cdot}875)^4}{12}\left[\left(\frac{b}{L}\right)^2 - \left(\frac{a}{L}\right)^2\right]. \tag{57}$$

Shown in Figure 2 are the non-dimensional rotation speeds ($\rho\omega^2L^2/E$) for which the first in-plane and first out-of-plane modes of a beam with a rectangular cross-section will have (rotating) natural frequencies in a 1:1 ratio as computed using equation (57). A family of curves is shown for non-dimensional cross-section dimensions a/L and $b/L = 0{\cdot}03$, $0{\cdot}04$ and $0{\cdot}05$. When the rotation speed vanishes, the natural frequencies have 1:1 ratios only when $a = b$. In the limit as $a/L \to 0$ for a fixed b/L, the model reduces to that of a rotating string in the out-of-plane direction.

It is important to note that the class of beams in which the height (a) is less than the base (b) of the cross-section (i.e., $I_y < I_z$) has a rotation speed at which the natural frequencies will be equal. This is in contrast to the stationary beam, which only has a 1:1 natural frequency ratio when the cross-section is a square ($a = b$). Note that Figure 2 is based upon a stationary beam mode. At high rotation speeds, a more accurate approximation can be obtained by using the rotating beam modes in equation (54).

6.2. TYPICAL RESPONSE CHARACTERISTICS

To illustrate characteristic behavior of this system, the following example is presented. The system parameters were chosen to match those of an experiment discussed in reference [13]. The beam is made of Lexan with density $\rho = 74{\cdot}913$ slugs/ft^3; Young's modulus, $E = 4{\cdot}968 \times 10^7$ psi; length, $L = 20{\cdot}0$ in and cross-sectional area dimensions, $a = 0{\cdot}8$ in $\times\, b = 1{\cdot}0$ in. The radius of the rigid body is $R = 3{\cdot}0$ in and its rotation speed is $\omega = 84{\cdot}3$ rad/s (805 rpm). The modal damping ratios are taken to be $\zeta_a = \zeta_b = \zeta_c = 0{\cdot}01$. From equations (30)–(31), the effective natural frequencies in the in-plane and out-of-plane directions are $\kappa_b = 1{\cdot}9827494$ and $\kappa_c = 1{\cdot}9822064$, respectively, making $\epsilon\sigma_2 = 5{\cdot}43 \times 10^{-4}$. In the figures to follow, solid (dashed) curves indicate stable (unstable) periodic responses obtained from the perturbation analysis. The circles indicate results obtained by numerically integrating the equations of motion (8)–(10).

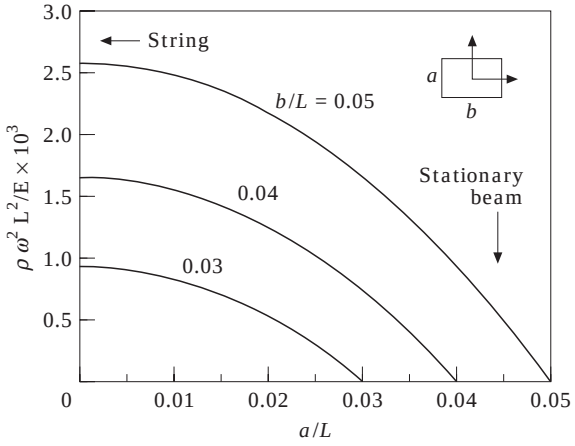

Figure 2. The curves indicate combinations of beam cross-sections ($a/L \times b/L$) and non-dimensional rotation rates squared ($\rho\omega^2L^2/E$), which cause the in-plane and out-of-plane natural frequencies to be in a 1:1 ratio.

Shown in Figure 3 is the out-of-plane response amplitude M_c as a function of excitation frequency for an excitation amplitude of $F = 2{\cdot}5$ lbf. This clearly displays the typical hysteresis region in the amplitude response diagram associated with non-linear deformations as discussed both theoretically and experimentally in references [14, 15] for the stationary beam. This response is a softening type and displays a saddle node bifurcations at $\Omega/\omega = 1{\cdot}8899$ (point A) and at $\Omega/\omega = 1{\cdot}9159$ (point B). At this low excitation level, only the out-of-plane (directly excited) mode responds.

Shown in Figures 4(a)–4(c) are the response amplitudes M_c (out-of-plane) and M_b (in-plane) as a function of excitation frequency for $F = 4{\cdot}0$ lbf. Consider the motion as the frequency is decreased from $\Omega/\omega = 2{\cdot}1$. Initially, only the one-degree-of-freedom response, M_c, exists. At $\Omega/\omega = 1{\cdot}9352$ (point A), the system undergoes a supercritical pitchfork bifurcation and a stable 1:1 internally resonant response is initiated while the one-degree-of-freedom response becomes unstable. As the excitation frequency continues to decrease, the magnitude of the in-plane motion grows and then levels off. At $\Omega/\omega = 1{\cdot}8523$ (point B), the system experiences a Hopf bifurcation and the 1:1 solution branch becomes unstable. Following the 1:1 response branch, it then exchanges stability at another Hopf bifurcation at $\Omega/\omega = 1{\cdot}7129$ (point C). As the in-plane motion continues to decrease, the system experiences a third Hopf bifurcation at $\Omega/\omega = 1{\cdot}6791$ (point D); see Figure 4(b). The unstable 1:1 response then vanishes at a sub-critical pitchfork bifurcation at $\Omega/\omega = 1{\cdot}6771$ (point E). The upper branch of the one-degree-of-freedom response is unstable until a Hopf bifurcation occurs at $\Omega/\omega = 1{\cdot}6732$ (point F). The upper branch exchanges stability at a saddle node point at $\Omega/\omega = 1{\cdot}6649$ (point G).

Now consider the response for increasing frequency beginning at $\Omega/\omega = 1{\cdot}6$. Only the one degree-of-freedom response exists. As the frequency increases, the directly excited modal amplitude M_c increases until a saddle node bifurcation occurs at $\Omega/\omega = 1{\cdot}8853$ (point H). The system then "jumps up" to the stable 1:1 response branch. Shortly, thereafter, a pitchfork bifurcation is encountered at $\Omega/\omega = 1{\cdot}9352$ (point A) and the one-degree-of-freedom motion is reestablished. Note, that in the frequency range, $1{\cdot}6649 < \Omega/\omega < 1{\cdot}6732$ (between points G and F) two stable one-degree-of-freedom responses coexist. A one-degree-of-freedom and a 1 : 1 internally resonant response coexist

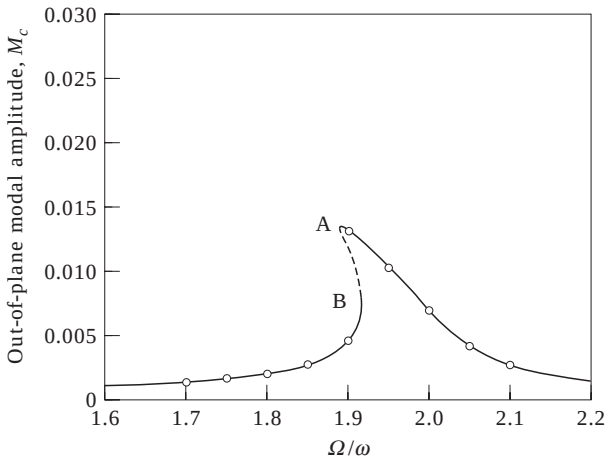

Figure 3. The out-of-plane modal amplitude (M_c, $M_b = 0$), versus the excitation frequency normalized with respect to the rotation speed (Ω/ω). The excitation amplitude is $F = 2{\cdot}5$ lbf. Due to the low forcing amplitude, there is insufficient energy to initiate a 1:1 internally resonant response.

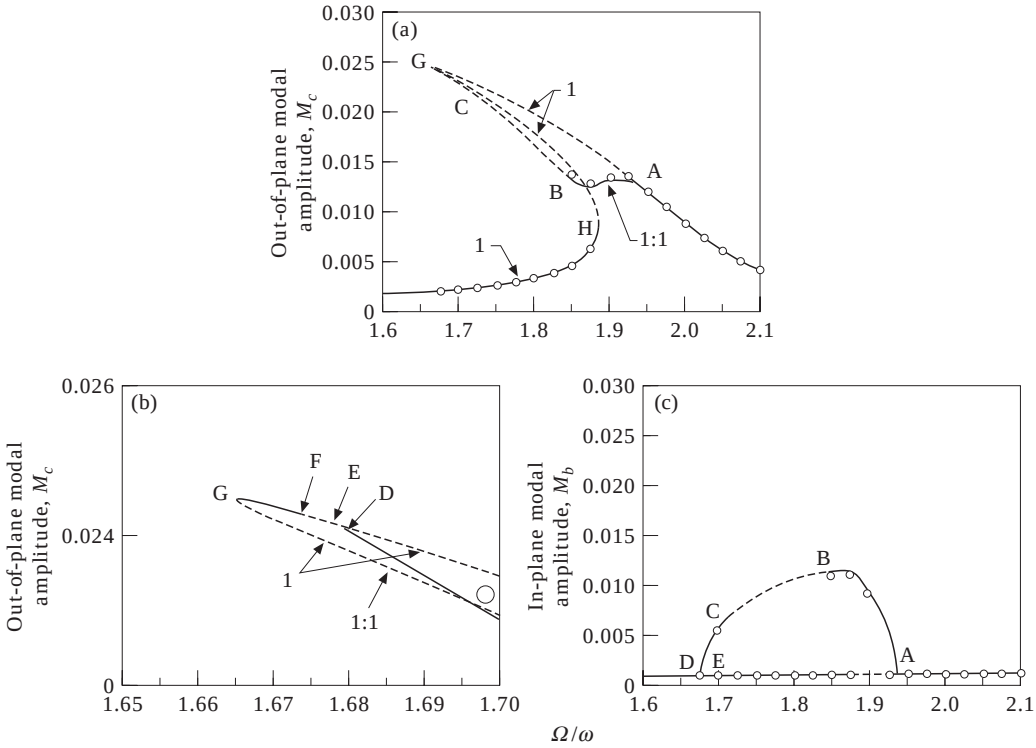

Figure 4. (a) The out-of-plane modal amplitude M_c versus the excitation frequency normalized with respect to the rotation speed (Ω/ω): the excitation amplitude is $F = 4{\cdot}0$ lbf. (b) This is an exploded view of Figure 4(a) in the region from C to G. (c) This is the in-plane motion corresponding to Figure 4(a): the excitation amplitude is $F = 4{\cdot}0$ lbf.

in the frequency ranges $1{\cdot}6791 < \Omega/\omega < 1{\cdot}7129$ (between points D and C) and $1{\cdot}8523 < \Omega/\omega < 1{\cdot}8853$ (between points B and H).

Shown in Figures 5(a) and 5(b) are the modal response amplitudes M_b and M_c at a higher excitation level of $F = 6{\cdot}0$ lbf. As the frequency is decreased from $\Omega/\omega = 2{\cdot}1$, the motion consists of a one-degree-of-freedom response in M_c ($M_b = 0$). At $\Omega/\omega = 1{\cdot}9365$ (point A), a supercritical pitchfork bifurcation occurs which initiates a stable 1:1 internally resonant response and the one-degree-of-freedom response loses stability. The 1:1 response exchanges stability at a saddle node bifurcation at $\Omega/\omega = 1{\cdot}7723$ (point B). The unstable 1:1 branch can then be traced into a Hopf bifurcation at $\Omega/\omega = 1{\cdot}8098$ (point C) where stability is again exchanged but only briefly as the response exchanges stability at a saddle node bifurcation at $\Omega/\omega = 1{\cdot}8132$ (point D). The 1:1 response branch then remains unstable.

Beginning at the low frequency end, $\Omega/\omega = 1{\cdot}6$, only the one-degree-of-freedom response is stable. As the frequency is increased, the out-of-plane response amplitude increases until a saddle node bifurcation is encountered at $\Omega/\omega = 1{\cdot}8509$ (point E). The response then "jumps up" to the stable 1:1 response branch. This branch remains stable until $\Omega/\omega = 1{\cdot}9365$ where the one-degree-of-freedom response is restabilized through the pitchfork bifurcation (point A). In the frequency range $1{\cdot}8098 < \Omega/\omega < 1{\cdot}8132$ (between points C and D), two 1:1 internally resonant responses and a one-degree-of-freedom response coexist.

It should be emphasized that the response described by M_b (in-plane motion) and M_c (out-of-plane motion) corresponds to steady state motions about a quasi-static deflection in the axial direction which arises from the (constant) centrifugal force field.

6.3. INITIATION OF THE PITCHFORK BIFURCATION

In the previous section, it was shown that the 1:1 internally resonant response will be initiated at a supercritical pitchfork bifurcation. The location of these bifurcation points depends on the system parameters and can be located in the system parameter space by considering the state equations governing the stability of the periodic solutions.

The eigenvalues of equation (53) are zero at a pitchfork bifurcation point. By setting the determinate of $[S]$ equal to zero, the points at which the 1:1 response solutions bifurcate from the one-degree-of-freedom responses may be obtained. This is done for various rotation speeds and aspect ratios in the $(F, \Omega/\omega)$ parameter plane.

The loci of bifurcation points for three different rotation speeds are shown in Figure 6. For now, consider only the case $\omega = 805$ rpm. Below $F = 2{\cdot}9$ lbf, there are no bifurcation points. This indicates that below this forcing level there is insufficient energy in the out-of-plane motion to trigger the in-plane motion. As the excitation level is gradually increased to $F \approx 4{\cdot}75$ lbf, bifurcations begin to occur at higher frequencies. As the

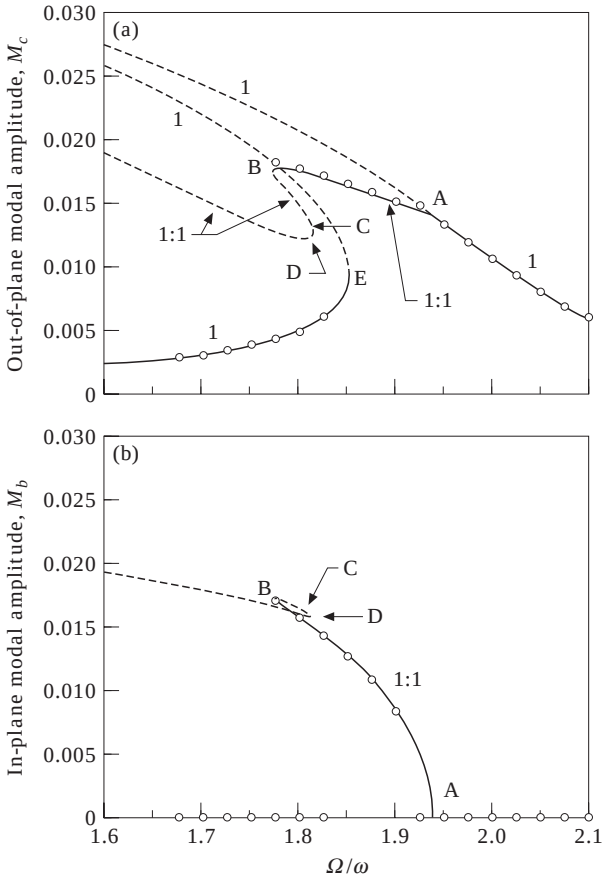

Figure 5. (a) The out-of-plane modal amplitude M_c versus the excitation frequency normalized with respect to the rotation speed (Ω/ω): the excitation amplitude is $F = 6{\cdot}0$ lbf. (b) This is the in-plane motion corresponding to Figure 5(a): the excitation amplitude is $F = 6{\cdot}0$ lbf.

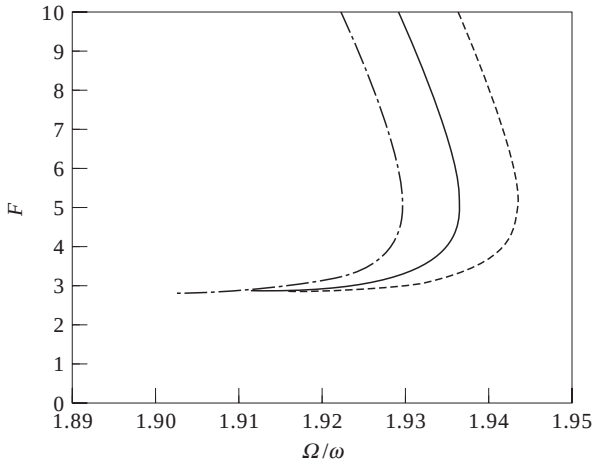

Figure 6. The parameter family corresponding to the onset of the pitchfork bifurcation initiating the 1:1 response for a fixed aspect ratio. In this case, $a/L = 0{\cdot}04$ and $b/L = 0{\cdot}05$. — · —, $\omega = 798$ rpm; —, $\omega = 805$ rpm; ----, $\omega = 812$ rpm.

excitation level is increased still further the curve bends to the left and the bifurcation frequency decreases. This "bending back" phenomenon which is encountered as F is increased would not be detectable if the perturbation scheme were limited to first non-linear order.

Similar trends are shown for two other rotation speeds, $\omega = 798$ rpm and $\omega = 812$ rpm. However, the absolute value of the bifurcation frequency is shifted to the left ($\omega = 798$ rpm) and to the right ($\omega = 812$ rpm) relative to the $\omega = 805$ rpm case. This indicates that at higher rotation speeds, more energy (greater excitation) is needed to initiate multi-degree-of-freedom responses.

Depicted in Figure 7 are the loci of pitchfork bifurcation points for three beams of different heights with a fixed width $b/L = 0{\cdot}05$ and rotation speed $\omega = 805$ rpm. First, consider the $a/L = 0{\cdot}04$ curve. Again, below $F = 2{\cdot}9$ lbf there are no bifurcation points

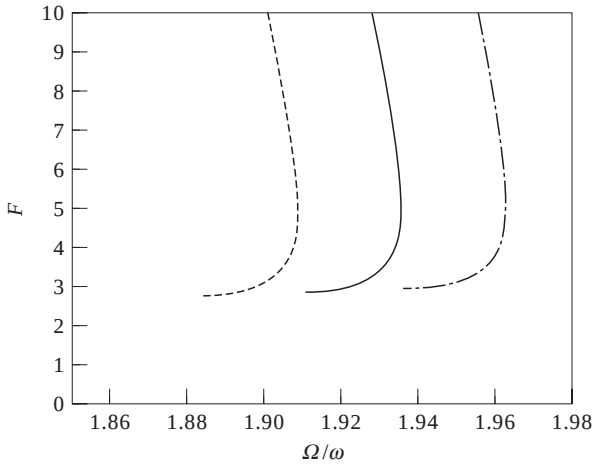

Figure 7. The parameter family corresponding to the onset of the pitchfork bifurcation initiating the 1:1 response for a fixed rotation rate. Here $b/L = 0{\cdot}05$ and $\omega = 850$ rpm. — · —, $a/L = 0{\cdot}03875$; —, $a/L = 0{\cdot}04$; ----, $a/L = 0{\cdot}04125$.

because of insufficient energy to excite the in-plane mode. Above this level of F, the point of bifurcation $(\Omega/\omega)_b$ initially increases with F. As the excitation level continues to increase past $F = 5$ lbf, the bifurcation frequencies begin to decrease. As observed in Figure 6, this "bending back" phenomenon is detectable only through a second order analysis.

Two other beam heights are shown in Figure 7: $a/L = 0{\cdot}03875$ and $a/L = 0{\cdot}04125$. The taller beam shifts the loci to the left, while the shorter beam shifts the loci to the right.

7. CONCLUSIONS

A three-dimensional non-linear continuum model that captures the effects of centrifugal stiffening, axial stretching and gyroscopic coupling is derived for a flexible, Euler–Bernoulli beam attached to a rigid body rotating at constant speed. Using a corresponding three-degree-of-freedom discrete model, modal coupling between lateral in-plane and out-of-plane motion is examined using a second order perturbation analysis. The occurrence of the one-to-one internally resonant response is shown to depend upon both the beam cross-section and the rate of rotation. This occurs for rectangular cross-sections, in which $b > a$, because centrifugal stiffening produces unequal changes in the in-plane frequencies as the beam rotates. This is in contrast with the stationary beam which may only experience a 1:1 response if the cross-section is square.

Typical response characteristics are presented which show the transition from a purely out-of-plane response (single degree of freedom) to a coupled in-plane/out-of-plane internally resonant response. Furthermore, it is shown that the 1:1 response is initiated by either a supercritical pitchfork bifurcation (for decreasing Ω/ω) or a saddle node bifurcation (for increasing Ω/ω).

Finally, the pitchfork bifurcation and its dependence on the excitation level and frequency are examined. Specifically, the parameter combinations which initiate this route to the coupled 1:1 response are determined in the excitation level F versus excitation frequency Ω/ω parameter space. The point of bifurcation is shown to vary considerably, particularly at low excitation levels.

ACKNOWLEDGMENTS

The authors would like to thank Professor David Peters of Washington University in St. Louis for his helpful comments. The work of the second author (C.L.) was performed under the auspices of the U.S. Department of Energy by the Lawrence Livermore National Laboratory under contract No. W-7405-ENG-48. The support of the New Technologies Engineering Division, LLNL, is gratefully acknowledged.

REFERENCES

1. D. H. Hodges and E. H. Dowell 1974 *NASA Technical Note D*-7818. Nonlinear equations of motion for the elastic bending and torsion of twisted nonuniform rotor blades.
2. J. C. Simo and L. Vu-Quoc 1986 *Transactions of the American Society of Mechanical Engineers*, *Journal of Applied Mechanics* **53**, 849–854. On the dynamics of flexible beams under large overall motions—the plane case: part I.
3. H. H. Yoo, R. R. Ryan and R. A. Scott 1995 *Journal of Sound and Vibration* **181**, 261–278. Dynamics of flexible beams undergoing overall motions.
4. K. R. V. Kaza and R. G. Kvaternik 1977 *American Institute of Aeronautics and Astronautics Journal* **15**(6), 871–874. Nonlinear flap–lag–axial equations of a rotating beam.
5. I. Sharf 1995 *Journal of Guidance*, *Control*, *and Dynamics* **18**(4), 882–890. Geometric stiffening in multibody dynamics formulations.

6. S. HANAGUD and S. SARKAR 1989 *Journal of Guidance, Control, and Dynamics* **12**(3) 438–441. Problem of the dynamics of a cantilever beam attached to a moving base.
7. T. R. KANE, R. R. RYAN and A. K. BANERJEE 1987 *Journal of Guidance, Control, and Dynamics* **10**, 139–151. Dynamics of cantilever beam attached to a moving base.
8. D. J. SEGALMAN and C. R. DOHRMANN 1996 *Journal of Vibration and Acoustics* **118**, 313–317. A method for calculating the dynamics of rotating flexible structures, part 1: derivation.
9. M. R. M. CRESPO DA SILVA and C. L. ZARETZKY 1990 *International Journal of Non-Linear Mechanics* **25**(2) 227–239. Non-linear modal coupling in planar and non-planar responses of inextensible beams.
10. A. G. HADDOW, A. D. S. BARR and D. T. MOOK 1984 *Journal of Sound and Vibration* **97**, 451–473. Theoretical and experimental study of modal interactions in a two degree of freedom system.
11. C. L. LEE and N. C. PERKINS 1995 *Nonlinear Dynamics* **8**, 45–63. Three-dimensional oscillations of suspended cables involving simultaneous internal resonances.
12. P. V. BAYLY and K. D. MURPHY 1998 *Journal of the Acoustical Society of America* (submitted). Coupling between dissimilar modes in an asymmetrically-forced string.
13. C. L. LEE, M. F. AL-SALEM and T. G. WOEHRLE 1998 *Journal of Applied Mechanics* (submitted). Free vibration of a cantilever beam attached to a rotating body.
14. W. Y. TSENG and J. DUGUNDJI 1970 *Journal of Applied Mechanics* **37**, 292–297. Nonlinear vibrations of a a beam under harmonic excitation.
15. W. Y. TSENG and J. DUGUNDJI 1971 *Journal of Applied Mechanics* **38**, 467–476. Nonlinear vibrations of a buckled beam under harmonic excitation.
16. Z. RAHMAN and T. D. BURTON 1989 *Journal of Sound and Vibration* **133**, 369–379. On higher order methods of multiple scales in non-linear oscillations—periodic steady state response.

APPENDIX A: PARTICULAR SOLUTIONS

The particular solutions at $O(\epsilon^2)$ are

$$\alpha_2 = \mathrm{i}v_{a1}\,\Gamma_1\,C_b\,\mathrm{e}^{\mathrm{i}\eta_b T_0} - \mathrm{i}v_{a1}\,\Gamma_1\,\bar{C}_b\,\mathrm{e}^{-\mathrm{i}\eta_b T_0} + \Gamma_2\,C_b^2\,\mathrm{e}^{\mathrm{i}2\eta_b T_0} + \Gamma_2\,\bar{C}_b^2\,\mathrm{e}^{-\mathrm{i}2\eta_b T_0} + \Gamma_3\,C_c^2\,\mathrm{e}^{\mathrm{i}2T_0} + \Gamma_3\,\bar{C}_c^2\,\mathrm{e}^{-\mathrm{i}2T_0} + (\Gamma_4\,C_b\,\bar{C}_b + \Gamma_5\,C_c\,\bar{C}_c),$$

$$\beta_2 = \mathrm{i}v_{b1}\,\Gamma_6\,C_a\,\mathrm{e}^{\mathrm{i}\eta_a T_0} + \mathrm{i}v_{b1}\,\Gamma_6\,\bar{C}_a\,\mathrm{e}^{-\mathrm{i}\eta_a T_0} + \Gamma_7\,C_a\,C_b\,\mathrm{e}^{\mathrm{i}(\eta_a+\eta_b)T_0} + \Gamma_8\,C_a\,\bar{C}_b\,\mathrm{e}^{\mathrm{i}(\eta_a-\eta_b)T_0} + \Gamma_8\,\bar{C}_a\,C_b\,\mathrm{e}^{-\mathrm{i}(\eta_a-\eta_b)T_0} + \Gamma_7\,\bar{C}_a\,\bar{C}_b\,\mathrm{e}^{-\mathrm{i}(\eta_a+\eta_b)T_0},$$

$$\gamma_2 = \Gamma_9\,C_a\,C_c\,\mathrm{e}^{\mathrm{i}(\eta_a+1)T_0} + \Gamma_{10}\,C_a\,\bar{C}_c\,\mathrm{e}^{\mathrm{i}(\eta_a-1)T_0} + \Gamma_{10}\,\bar{C}_a\,C_c\,\mathrm{e}^{-\mathrm{i}(\eta_a-1)T_0} + \Gamma_9\,\bar{C}_a\,\bar{C}_c\,\mathrm{e}^{-\mathrm{i}(\eta_a+1)T_0},$$

where

$$\Gamma_1 = \frac{-1}{\eta_a^2-\eta_b^2}\frac{\eta_b}{\kappa_c^2}, \qquad \Gamma_6 = \frac{-1}{\eta_b^2-\eta_a^2}\frac{\eta_a}{\kappa_c^2},$$

$$\Gamma_2 = \frac{-1}{\eta_a^2-4\eta_b^2}\frac{A_4}{\kappa_c^2}, \qquad \Gamma_7 = \frac{-1}{-(\eta_a+\eta_b)^2+\eta_b^2}\frac{B_3}{\kappa_c^2},$$

$$\Gamma_3 = \frac{-1}{\eta_a^2-4}\frac{A_5}{\kappa_c^2}, \qquad \Gamma_8 = \frac{-1}{-(\eta_a-\eta_b)^2+\eta_b^2}\frac{B_3}{\kappa_c^2},$$

$$\Gamma_4 = \frac{-2}{\eta_a^2}\frac{A_4}{\kappa_c^2}, \qquad \Gamma_9 = \frac{-1}{1-(\eta_a+1)^2}\frac{C_2}{\kappa_c^2},$$

$$\Gamma_5 = \frac{-2}{\eta_a^2}\frac{A_5}{\kappa_c^2}, \qquad \Gamma_{10} = \frac{-1}{1-(\eta_a-1)^2}\frac{C_2}{\kappa_c^2}.$$

APPENDIX B: ELEMENTS OF MATRIX [S]

The elements of the matrix [S], which dictates the stability of lateral oscillations, are given by

$$S_{11} = \frac{-(2\zeta_b\,\omega_b(\Omega/\omega))\eta_b + \frac{1}{4}\,B_3\,\Gamma_3\,M_c^2\sin(\theta) + \frac{1}{4}\,B_4\,M_c^2\sin(\theta)}{2\kappa_c^2\,\eta_b},$$

$$S_{12} = \frac{\begin{array}{c}[(\Omega/\omega)^2 - \kappa_c^2]\eta_b^2 + A_1\,B_1(\Omega/\omega)^2\eta_b\,\Gamma_1 - B_3\,(\Gamma_4 + \Gamma_2) \\ \times\, M_b^2\,/4 - B_3\,M_c^2\,[\Gamma_5 - \Gamma_3\cos(\theta)]/4 - 3B_5\,M_b^2\,/4 - B_4\,M_c^2\,[2 - \cos(\theta)]/4\end{array}}{2\kappa_c^2\,\eta_b},$$

$$S_{13} = \frac{B_3\,\Gamma_3\,M_b\,M_c\sin(\theta) + B_4\,M_b\,M_c\sin(\theta)}{4\kappa_c^2\,\eta_b},$$

$$S_{14} = \frac{B_3\,\Gamma_3\,M_b\,M_c\cos(\theta) + B_4\,M_b\,M_c\cos(\theta)}{4\kappa_c^2\,\eta_b},$$

$$S_{21} = \frac{\begin{array}{c}[(\Omega/\omega)^2 - \kappa_c^2]\eta_b^2 + A_1\,B_1\,(\Omega/\omega)^2\eta_b\,\Gamma_1 - 3B_3\,(\Gamma_4 + \Gamma_2)M_b^2/4 - B_3\,M_c^2 \\ \times\,[\Gamma_5 + \Gamma_3\cos(\theta)]/4 - 9B_5\,M_b^2\,/4 - B_4\,M_c^2\,[2 - \cos(\theta)]/4\end{array}}{-2\kappa_c^2\,\eta_b},$$

$$S_{22} = \frac{(2\zeta_b\,\omega_b\,(\Omega/\omega))\eta_b + \frac{1}{4}\,B_3\,\Gamma_3\,M_c^2\sin(\theta) + \frac{1}{4}\,B_4\,M_c^2\sin(\theta)}{-2\kappa_c^2\,\eta_b},$$

$$S_{23} = \frac{-B_3\,M_b\,M_c\,(2\Gamma_5 + \Gamma_3\cos(\theta)) - B_4\,M_b\,M_c\,(2 + \cos(\theta))}{-4\kappa_c^2\,\eta_b},$$

$$S_{24} = \frac{-B_3\,\Gamma_3\,M_b\,M_c\sin(\theta) - B_4\,M_b\,M_c\sin(\theta)}{4\kappa_c^2\,\eta_b},$$

$$S_{31} = \frac{-C_2\,\Gamma_2\,M_b\,M_c\sin(\theta)\,(C_2 + C_3)}{4\kappa_c^2},$$

$$S_{32} = \frac{-C_2\,\Gamma_2\,M_b\,M_c\cos(\theta)\,(C_2 + C_3)}{4\kappa_c^2},$$

$$S_{33} = \frac{-(2\zeta_c\,\omega_c\,(\Omega/\omega)) - M_b^2\,(C_2\,\Gamma_2\sin(\theta)/4 + C_3\sin(\theta))/4}{2\kappa_c^2},$$

$$S_{34} = \frac{\begin{array}{c}[(\Omega/\omega)^2 - \kappa_c^2] - C_2\,(\Gamma_5 + \Gamma_3)M_c^2/4 - C_2\,M_b^2 \\ \times\,[\Gamma_4 - \Gamma_2\cos(\theta)]/4 - 3C_4\,M_c^2/4 - C_3\,M_b^2\,[2 - \cos(\theta)]/4\end{array}}{2\kappa_c^2},$$

$$S_{41} = \frac{-M_b\,M_c\,(C_2\,\Gamma_4 + 2C_3) + M_b\,M_c\,(\Gamma_2\,C_2 + C_3)\cos(\theta)}{-4\kappa_c^2},$$

$$S_{42} = \frac{M_b\,M_c\sin(\theta)\,(C_2\,\Gamma_2 + C_3)}{-4\kappa_c^2},$$

$$S_{43} = \frac{\begin{array}{c}[(\Omega/\omega)^2 - \kappa_c^2] - 3C_2\,(\Gamma_5 + \Gamma_3)M_c^2/4 - C_2\,M_b^2\,[\Gamma_4 + \Gamma_2\cos(\theta)]/4 - 9C_4\,M_c^2/4 \\ -\,C_3\,M_b^2\,[2 + \cos(\theta)]/4\end{array}}{-\,2\kappa_c^2},$$

$$S_{44} = \frac{-(2\zeta_c\,\omega_c\,(\Omega/\omega)) - M_b^2\sin(\theta)\,(C_2\,\Gamma_2 + C_3)/4}{-\,2\kappa_c^2}.$$